Pergamon

Geochimica et Cosmochimica Acta, Vol. 68, No. 21, pp. 4395–4403, 2004

0016-7037/04 $30.00 + .00

doi:10.1016/j.gca.2004.03.016

Mineralogical and isotopic properties of inorganic nanocrystalline magnetites

Damien Faivre,[1,*] Pierre Agrinier,[2] Nicolas Menguy,[3] Pierpaolo Zuddas,[1,4] Katavut Pachana,[1] Alexandre Gloter,[5] Jean-Yves Laval,[6] and François Guyot[3]

[1]Laboratoire de Géochimie des Eaux, CNRS UMR 7047, Université Paris 7 (UP7) and Institut de Physique du Globe de Paris (IPGP), case postale 7052, 2 place Jussieu, 75251 Paris cedex 05, France
[2]Laboratoire de Géochimie des Isotopes Stables, CNRS UMR 7047, UP7 and IPGP, 4 place Jussieu, 75251 Paris cedex 05, France
[3]Laboratoire de Minéralogie et Cristallographie de Paris, CNRS UMR 7590, Universités Paris 6, UP 7 & IPGP, 4 place Jussieu, 75251 Paris cedex 05, France
[4]PaléoEnvironnement & PaléobioSphère, CNRS UMR 5125, Université Lyon 1, 43 bd du 11 Novembre 1918, 69622 Villeurbanne cedex, France
[5]Laboratoire de Physique des Solides, CNRS UMR 8502, Université Paris-Sud, 91405 Orsay cedex, France
[6]Laboratoire de Physique des Solides, CNRS UPR 5, ESPCI, 75231 Paris cedex 05, France

(*Received October* 16, 2003; *accepted in revised form March* 1, 2004)

Abstract—Inorganic magnetite nanocrystals were synthesized in an aqueous medium at 25°C, atmospheric pressure, ionic strength of 0.1 M, oxygen fugacity close to 0, and under controlled chemical affinity, which was maintained constant during an experiment and varied between different experiments. The total concentration of iron in the initial solutions, with Fe(III)/Fe(II) ratios of 2, was varied in order to measure the role of this parameter on the reaction rate, particle morphology, and oxygen isotopic composition. The reaction rates were followed by a *p*Hstat apparatus. The nature and morphology of particles were studied by transmission electron microscopy and electron energy loss spectroscopy. Fractionation factors of oxygen isotopes were determined by mass spectrometry after oxygen extraction from the solid on BrF_5 lines. At low total iron concentrations, goethite and poorly crystalline iron oxides were observed coexisting with magnetite. At higher concentrations, euhedral single crystals of pure magnetite with an average characteristic size of 10 nm were formed, based on a first-order rate law with respect to total iron concentration. These results confirm that, under high supersaturation conditions, low-temperature inorganic processes can lead to the formation of well-crystallized nanometric magnetite crystals with narrow size distribution. The observed oxygen isotope fractionation factor between magnetite crystals and water was of 0–1‰, similar to the fractionation factor associated with bacterially produced magnetite. We suggest that the solution chemistry used in this study for inorganic precipitation is relevant to better understanding of magnetite precipitation in bacterial magnetosomes, which might thus be characterized by high saturation states and *p*H.

1. INTRODUCTION

Iron oxides formed at low temperature in aqueous media record natural processes of fundamental geochemical and biogeochemical importance (Anbar, 2001; Anbar, 2004; Baeuerlein, 2000; Bazylinski, 1999; Kirschvink and Hagadorn, 2000; Krumbein, 1983; Newman, 2001). Among those oxides, nanometric magnetites have generated numerous studies. Magnetotactic bacteria found in 1975 (Blakemore, 1975; Blakemore et al., 1979; Frankel and Blakemore, 1979) are important components of the oxic to anoxic transition zone in natural settings (Bazylinski et al., 1995; Mortimer and Coleman, 1997) and are found in sediments. They have been related to paleomagnetic studies (Chang and Kirschvink, 1989; Kirschvink, 1982; Kirschvink and Chang, 1984; Moskovitz et al., 1993; Vali et al., 1987; Vali and Kirschvink, 1989). Magnetite nanoparticles have been found in the ALH 84001 meteorite and are therefore important in discussions about possible extraterrestrial life (McKay et al., 1996; Romanek et al., 1994). The debate about the possible biogenic origin of the crystals (Barber and Scott, 2002; Bradley et al., 1997; Frankel and Buseck, 2000; Friedmann et al., 2001; Thomas-Keprta et al., 2000; Thomas-Keprta et al., 2001) emphasizes that bacterial magnetites cannot always be obviously differentiated from those produced abiotically (Devouard et al., 1998; Golden et al., 2001).

Extensive studies in the literature have reported nanometric-size bacterial (intracellular and extracellular) magnetites (e.g., see references in Baeuerlein, 2000 or Schüler and Frankel, 1999). An increasing number of studies have reported magnetites formed inorganically in aqueous systems (Cornell and Schwertmann, 1996; Jolivet et al., 1994; Mann et al., 1989; Qu et al., 1999; Regazzoni et al., 1981; Schwertmann and Cornell, 1991; Tronc et al., 1992; Vayssières, 1995; Vayssières et al., 1998), principally because of the increasing interest for nanoscience (Hochella Jr., 2002). Studies in inorganic aqueous media have emphasized the role of *p*H and ionic strength on the precipitation of the magnetite nanocrystals and on their dimensions.

Furthermore, studies of magnetites will be important in the developing field of isotopic studies of iron. Since Mandernack et al. (1999) reported the first study of iron isotopes on intracellular magnetite, different groups have shown the existence of a fractionation, either by biologic (Beard et al., 2003; Brantley et al., 2001) or nonbiologic (Bullen et al., 2001; Roe et al., 2003) processes. More conventional oxygen isotopes studies are also important (Fortier et al., 1995; Mandernack et al., 1999; O'Neil and Clayton, 1964; Zhang et al., 1997) because the quartz–magnetite pair has a large isotopic fractionation and therefore provides a sensitive isotopic geothermometer.

* Author to whom correspondence should be addressed (faivre@ipgp.jussieu.fr).

Table 1. Summary of measurements as a function of TIC[a].

Sample #	TIC (mol · L^{-1})	Phases observed	$\delta^{18}O_s$ (‰)	$\delta^{18}O_w$ (‰)	$10^3 \ln \alpha_{s\text{-}w}$	R_m (μmol min^{-1})	log Ω
1	0.003	Go + Io	n.d.	n.d.	n.d.	n.d.	71.7
2	0.009	Go + Io + Mt	−1.15 −1.25	−6.65 −6.65	5.52 5.42	1.54	76.7
3	0.018	Io + Mt	−3.32 −3.33	−6.59 −6.59	3.29 3.28	2.50	79.8
4	0.030	Mt	−6.30 −6.25	−6.64 −6.64	0.34 0.39	4.83	82.0
5	0.060	Mt	−6.88 −6.71	−6.84 −6.84	−0.04 0.13	9.85	84.9
6	0.090	Mt	−5.92 −5.83	−6.71 −6.71	0.80 0.89	14.48	86.6
7	0.120	Mt	−6.98 −7.37 −6.91	−6.74 −6.74 −6.74	−0.24 −0.63 −0.17	19.74	87.8
8	0.150	Mt	−6.60 −6.25 −6.72	−6.55 −6.55 −6.55	−0.05 0.30 −0.17	24.84	88.8
9	0.180	Mt	−6.13 −6.44	−6.69 −6.69	0.56 0.25	28.33	89.6

TIC = total iron concentration.

[a] Phases observed are goethite (Go), poorly crystallized iron oxides or hydroxides (Io) and magnetite (Mt). Results of isotope analyses are given as δ values for the solid and the water: $\delta^{18}O_s$, $\delta^{18}O_w$ respectively and as fractionation factors, $10^3 ln\ \alpha_{s\text{-}w}$, measured between the solid iron oxide phase and the solution. Each measurement has been at least duplicated. The two or three measured values are given in the column. Reaction rates, R_m, are given as the consumption rate of hydroxyl ions. Supersaturations (log Ω) are calculated using the solution chemistry code EQ3NR (Wolery, 1979).

The aim of the present study is to link the properties of abiotically precipitated crystals with their formation conditions and to investigate their oxygen isotopic signature at different supersaturation states of the solution. We therefore investigate the role of the saturation state in the solution and its effect on (1) the mineralogy of the precipitated crystals, (2) the reaction rates of the precipitation, and (3) the magnetite–water oxygen isotopic fractionation factor. We have thus studied the morphology, size, crystallographic characteristics, and oxygen isotopic compositions of crystals of magnetite of nanometric sizes, made abiotically, using different initial saturation states of the aqueous solution in which they were synthesized at normal conditions of pressure and temperature. The method of synthesis given in Vayssières et al. (1998) which enables the formation of magnetite at constant chemical affinity conditions was followed. The inorganically produced magnetite nanoparticles were analyzed by transmission electron microscopy (TEM) to determine their structure and by mass spectrometry for their oxygen isotopic compositions.

2. MATERIAL AND METHODS

2.1. Synthesis of Magnetite

Magnetite precipitation experiments were carried out by co-precipitation of ferrous and ferric ions in aqueous solution following a previously developed methodology (Vayssières, 1995) given by:

$$2\ Fe^{3+} + Fe^{2+} + 4\ H_2O \rightarrow Fe_3O_4 + 8\ H^+ \quad (1)$$

Equation 1 is a mass balance expression without any connection to an actual mechanism which most likely involves intermediate species both in solution and in the solid state. 50 mL of a solution (*p*H = 1.25) containing dissolved $FeCl_2$ and $FeCl_3$ in the stoichiometric ratio of the solid (Fe(III)/Fe(II) = 2) were added to 500 mL of sodium nitrate $NaNO_3$ solution at a rate of 0.5 mL per minute using an automatic pump (Metrohm 776 Dosimat). The ionic strength of the medium was fixed at I = 0.1 mol L^{-1} by the sodium nitrate solution. The precipitation cell was held at a constant temperature of 25 ± 0.5 °C. All solutions were previously boiled and carefully deoxygenated with nitrogen, which was continuously bubbling during the experiment to avoid Fe(II) oxidation. The *p*H of the medium was kept constant at *p*H = 10.5 ± 0.05 by addition of a 0.1 mol L^{-1} sodium hydroxide solution using a commercial *p*Hstat (Metrohm 718 STAT Titrino, calibration with Schott buffer solutions: *p*H 7.0 and 10.0 at 25°C). The *p*H was monitored with a *p*Hmeter, integrated in the *p*Hstat, with a Metrohm (6.0203.100, 3 mol L^{-1} KCl) combined electrode. Calibrations were done using Schott buffer solutions: *p*H 7.0 and 10.0 at 25°C. Total iron concentrations (TIC) in sampled aliquots of solutions were measured with graphite furnace atomic absorption spectroscopy (GFAAS) within an error of ±10%. As the reaction proceeds, sodium hydroxide is added automatically to the medium to maintain a constant *p*H, which allows the monitoring of the mean precipitation rate R_m (in μmol min^{-1}) according to:

$$R_m = \frac{1}{8}\frac{\Delta[OH^-]_{cor}}{\Delta t} \quad (2)$$

where $\Delta[OH^-]_{cor}$ is the total quantity of sodium hydroxide (in μmol) added during the precipitation time Δt (in min) and the 1/8 coefficient derives from the stoichiometric coefficient of the proton in Eqn. 1. Because the initial iron solution is maintained under acidic conditions to prevent precipitation of Fe (III), a correction volume is calculated (33.3 mL), which is the volume of 0.1 mol L^{-1} sodium hydroxide necessary for bringing the iron-bearing solution to a *p*H of 10.5. This volume is not used for the precipitation reaction and is therefore not included in the calculation of the mean reaction rate.

The experiments have been carried out under large supersaturation conditions with respect to magnetite precipitation. The solution supersaturation can be evaluated by calculating the initial chemical activity of reaction (1) using the solution chemistry code EQ3NR (Wolery, 1979), as reported in Table 1. The uncertainty associated with the solubility constant of magnetite is illustrated by the scattered values found in the literature (Cornell and Schwertmann, 1996; Michard, 1989; Sweeton and Baes Jr., 1970). This uncertainty will affect the value of log Ω by less than two log units, thus leaving unchanged the main point that all the experiments were carried under initial large supersaturations (Table 1). In the different experiments, the concentration of the added Fe^{2+} and Fe^{3+}-bearing solutions were changed to

explore the effect of this parameter. After injecting iron-bearing solution into the basic medium, magnetite precipitation occurs rapidly; the actual amounts of Fe^{2+} and Fe^{3+} in solution at a given time are thus difficult to determine. However, since the iron solution is added at a constant rate, a steady state is reached, characterized by a constant chemical affinity for the reaction (Vayssières et al., 1998). The saturation state of the experiment is thus well described by the TIC in the initial iron-bearing solution.

2.2. Analyses

2.2.1. Transmission electron microscopy

The precipitated crystals were characterized by TEM on a Jeol 2010 F operated at 200 kV, coupled with an energy-dispersive X-ray spectrometer (EDX) chemical analyzer (PGT-PRISM 2000, associated with IMIX software, with probe size of 1 nm, acquisition time of 300 s). Samples were prepared by two methods leading to consistent results. In the first method, a drop of the solution containing magnetite nanoparticles was directly deposited onto a copper mesh grid covered with a carbon film. After 10 s, the drop was removed and the grid was allowed to dry. In the second method, a solution containing precipitated magnetite particles was carefully washed after precipitation and evaporated under vacuum the following night. Particles were then placed in ethanol, and a drop of this mixture was placed onto the copper mesh grid for TEM analysis. The only difference observed between the two types of preparation was the presence, in the first case, of sodium nitrate crystals which were completely absent in the second case. Particle sizes were analyzed using standard analytical software for processing digitized electron microscopy images (Gatan DigitalMicrograph, Scion Image and CaRIne Cristallography [Monceau and Boudias, 1996]). Additional measurements were carried out by electron energy-loss spectroscopy (EELS) on a dedicated scanning transmission electron microscope VG HB005 equipped with a cold field emission gun providing a high energy resolution (0.6 eV) and a high spatial resolution (0.7 nm).

2.2.2. Analyses of oxygen isotopes

Analyses of oxygen isotopic compositions were performed on BrF_5 lines (Clayton and Mayeda, 1963). Solutions with precipitated magnetites were carefully washed after precipitation and evaporated under vacuum the following day. As revealed by Yapp (1987) and confirmed later by Bao and Koch (1999), these are crucial steps for obtaining reliable $\delta^{18}O$ for fine-grained, low-temperature precipitates. In our case, the oxygen isotopic signal might be modified by salts used to maintain ionic strength. Nitrate salts were always completely removed from samples to be analyzed for isotopes, as checked by TEM. Nearly 20 mg of solid material were necessary for each analysis. The solids were introduced in Ni tubes where they were preheated at 150°C under vacuum for 4 h to remove adsorbed water from the sample and then reacted with BrF_5 to form oxygen by the following reaction:

$$Fe_3O_4 + 4\ BrF_5 \rightarrow 2\ O_2 + 4\ BrF_3 + 2\ FeF_3 + \ FeF_2 \qquad (3)$$

The reaction, at 650°C, was done with an excess of BrF_5 (nearly five times greater than the necessary stoichiometry) to ensure that all iron oxides had reacted. Oxygen was separated from other gases by passage in liquid nitrogen traps that retained other volatile gases by condensation. In the following step, oxygen itself was trapped on a cooled zeolite (77 K), quantified to calculate the yield of the isotopic analyses, and finally transferred to the mass spectrometer (VG Optima) where intensities associated to the ions of masses 32 and 34 were measured. Yields are calculated as the ratio of the experimental yield on the theoretical yield. 8.63 μmol of O_2/mg of Fe_3O_4 are theoretically obtained based on the prefect gas law. Experiments with yields greater than 90% were accepted, whereas the others were rejected. Repetitive analyzes of NBS 28 (quartz, $\delta^{18}O = 9.35 \pm 0.11‰$, $n = 10$) and Circe 93 (basaltic glass from midoceanic ridge, $\delta^{18}O = 5.72 \pm 0.13‰$, $n = 25$) were used as calibration procedure with an overall procedure to overall errors of $\pm 0.2‰$.

The $\delta^{18}O$ of the water, before and after magnetite precipitation, were determined by CO_2-H_2O equilibration. One or two drops of 100% H_3PO_4 were previously added to the solutions to neutralize the alkaline media used for precipitation.

3. RESULTS AND DISCUSSION

3.1. Mineralogy and Precipitation Kinetics

3.1.1. Mineralogy

Syntheses were carried out using stock solutions with varying TIC from 3×10^{-3} to 180×10^{-3} mol L^{-1}. Some typical TEM observations are shown in Figure 1. Electron diffraction studies and EDX analyses show that for concentrations of less than 6×10^{-3} mol L^{-1} (sample #1), goethite particles (α-FeOOH) coexisting with poorly crystallized iron oxides and hydroxides are obtained instead of magnetite. The goethite crystals form star-shaped objects with characteristic elongated morphologies (Fig. 1a). Multidomain goethite twinned crystals have been commonly described (Cornell and Schwertmann, 1996). Poorly crystallized iron oxides and hydroxides appear as a matrix (Fig. 1b). With increasing TIC, small magnetite particles appear, coexisting with goethite crystals and poorly crystallized iron oxides and hydroxides (Fig. 1a,b). For TIC exceeding 30×10^{-3} mol L^{-1}, magnetite is the only phase observed (Fig. 1c). Crystals are single crystalline magnetites with euhedral shapes (Fig. 1d).

Electronic diffraction data do not allow for the facile differentiation of magnetite and maghemite. EELS spectra on the nanoparticles, however, demonstrate that the spinel particles observed here are not maghemite but magnetite. The EELS O-K edge measured for this iron oxide is displayed in Figure 2b and exhibits the main fine structures expected for a magnetite sample (Kendelewicz et al., 2000b). In particular, the shoulder at the high-energy side of the O-K prepeak (labelled B in Fig. 2b) has been systematically reported in X-ray absorption spectroscopy (XAS) and in high-energy resolved EELS experiments on magnetite. The O-K edge for maghemite has been less well studied. It can be noticed, however, that peaks B and D (Fig. 2b) have been reported rarely or with weaker intensity (see for instance, Blake et al., 1998). The Fe $L_{2,3}$ EELS spectrum of the observed nanoparticles is presented in Figure 2a. The Fe $L_{2,3}$ from a reference Fe^{3+} hematite sample, acquired on the same equipment, is also exhibited. Previous XAS and EELS works have demonstrated that the Fe $L_{2,3}$ fine structure is primarily governed by the valence state. Indeed, our α-Fe_2O_3 reference (hematite) closely resembles the already published spectra for a γ-Fe_2O_3 (maghemite) (Kendelewicz et al., 2000a). On the other hand, the Fe $L_{2,3}$ EELS spectra obtained on the iron oxide nanoparticles do not exhibit the features of a predominantly Fe^{3+} compound but show almost featureless $L_{2,3}$ lines. This absence of remarkable fine structures has already been shown for reference magnetite (Crocombette et al., 1995; Kendelewicz et al., 2000b; Schedin et al., 2000). It is interpreted as the result of a complex electronic environment involving mixed valences and some degree of covalent bonding (Crocombette et al., 1995; Kendelewicz et al., 2000b; Schedin et al., 2000). Such effects are not involved in both hematite and maghemite in which fine structures are thus normally present.

A statistical analysis of the magnetite crystal sizes has been carried out in five experiments. Particle sizes have been determined by image analysis on TEM pictures. The mean magnetite

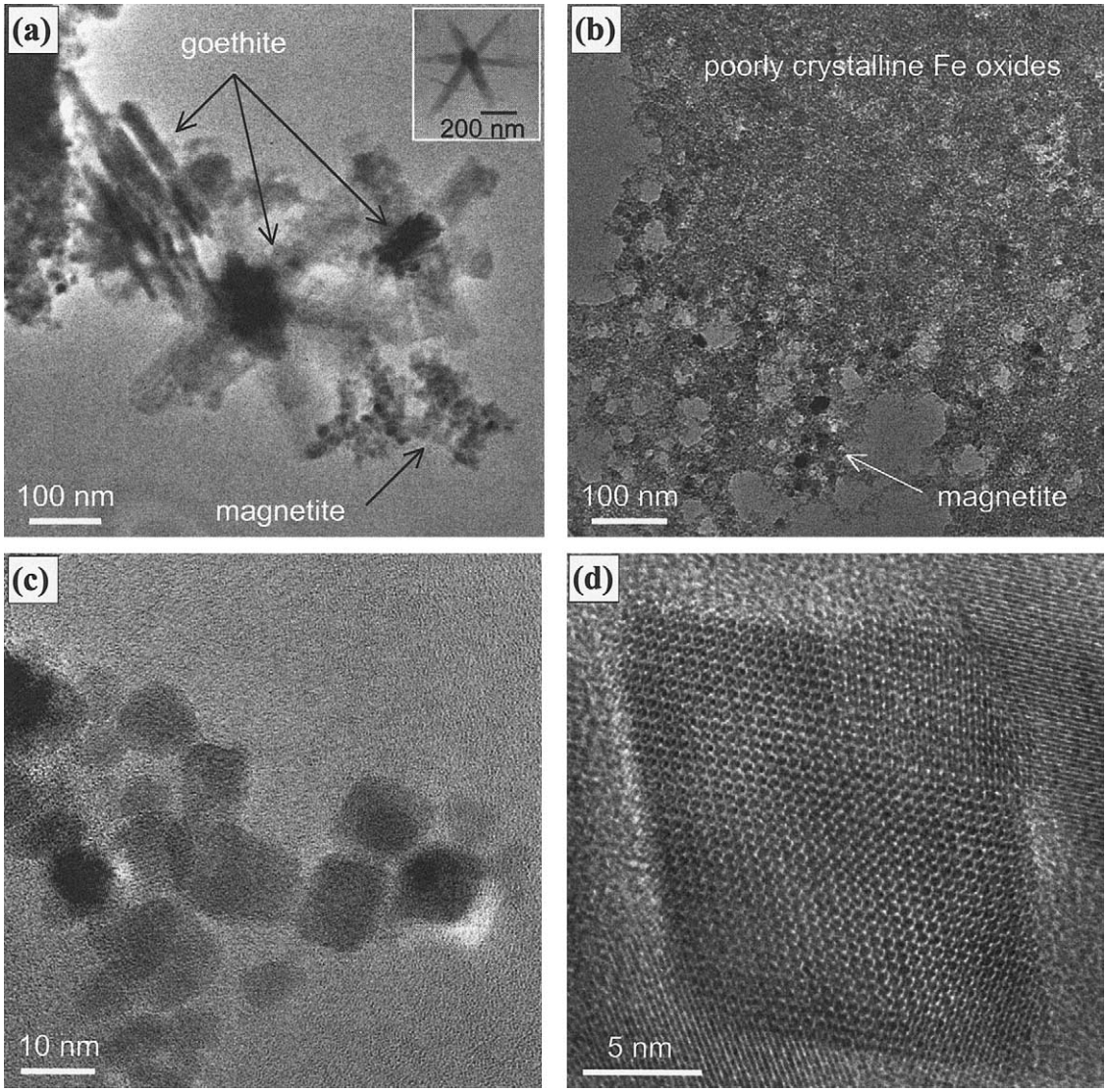

Fig. 1. TEM images of synthesized iron oxides particles formed at different values of TIC. (a) TEM image of goethite and magnetite generated from an experiment with TIC = 0.009 mol.L^{-1}. Inset: star-like morphology of goethite crystals. (b) TEM image from an experiment with TIC = 0.018 mol.L^{-1} showing magnetite crystals (appearing in dark contrast) embedded in a matrix of poorly organized iron oxide. (c) TEM image from a group of magnetite particles generated in an experiment with TIC = 0.060 mol.L^{-1} (only magnetite crystals are observed). (d) TEM image of a magnetite particle from an experiment with TIC = 0.180 mol.L^{-1}. Octahedral and well-crystallized crystals are systematically observed. The apparent defect structure visible in the upper part of the particle is an artefact due to an overlapping particle.

particle sizes are 10.3 (σ = 0.7), 10.7 (σ = 0.7), 10.1 (σ = 0.6), 10.1 (σ = 0.6), and 11.1 nm (σ = 0.8 nm) for samples # 2, 3, 5, 7, and 9, respectively (σ represents one standard deviation on the average value). A size distribution histogram merging measurements of the five aforementioned samples is given in Figure 3. No detectable effect of the investigated range of TIC on the dimension of particles is thus observed in the investigated range of TIC. The sizes of low-temperature magnetites have been analyzed in previous studies (Devouard et al., 1998; Jolivet et al., 1992; McCartney et al., 2001; Regazzoni et al., 1981; Taylor et al., 2001; Thomas-Keprta et al., 2000; Thomas-Keprta et al., 2001; Vayssières, 1995; Vayssières et al., 1998). Using higher ionic strengths and smaller reactors (pH = 10.5 to 13; I = 0.5 to 3 mol L^{-1} and v_{Fe} = 2.5 mL), Vayssières (1995) and Vayssières et al. (1998) obtained similar results as in the present study: they found no variations in crystal dimension for TIC changing from 0.075 to 3.0 mol L^{-1}. At pH = 10.5 and I = 0.5 mol L^{-1}, they report mean particle size of 9 nm for TIC of 0.75, 1.5, and 3 mol L^{-1}, in good agreement with the present study. The measured size distribution is also consistent with that measured under different but comparable experimental conditions by Jolivet et al. (1992). Devouard et al. (1998) used a completely different pathway for synthesizing small sized magnetites, as described in Cornell and Schwertmann (1996) and Schwertmann and Cornell (1991). With this method, Fe^{2+} is oxidized at 90°C for 60 min in a 3.33 mol L^{-1} KOH and 0.27 mol L^{-1} KNO_3 medium. They observed inorganic magnetites or maghemites ranging from 20 to 120 nm, with a great

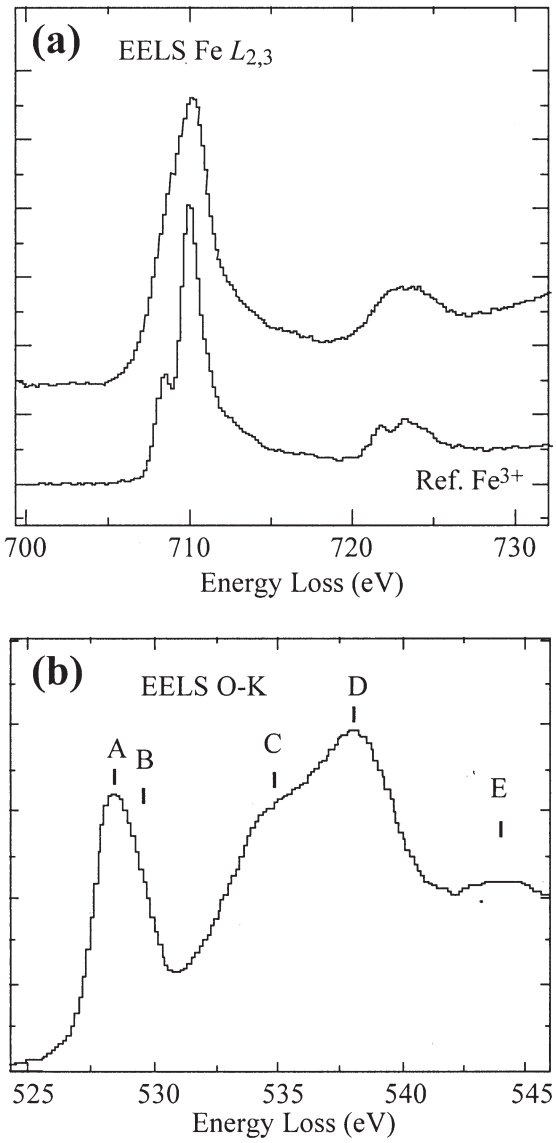

Fig. 2. EELS spectra. Fe $L_{2,3}$ (a) and O-K (b) edges of magnetites from an experiment with TIC: 0.180 mol.L^{-1}. Features labeled by letters are discussed in text. An Fe $L_{2,3}$ reference spectrum for a pure Fe^{3+} phase (hematite) acquired under the same conditions is given (top diagram: ref Fe^{3+}).

majority being in the 20–80-nm interval. The sizes are much larger than in the present study, but the ionic strength, nature of ions in solution, and the strong variation in thermodynamic activities during reaction make the two synthetic pathways difficult to compare. Mann and Hannington (1987) reported a method in which magnetite, goethite, and ferrihydrite were respectively precipitated within unilamellar phosphatidylcholine vesicles of ca. 30 nm. Magnetite crystals precipitated from Fe(II)/Fe(III) intravesicular solutions containing NaOH, after 30 min of aging, were spherical and 2 to 6 nm in diameter. Again, the differences due to the presence of the vesicles make the sizes difficult to compare with those measured in the present study.

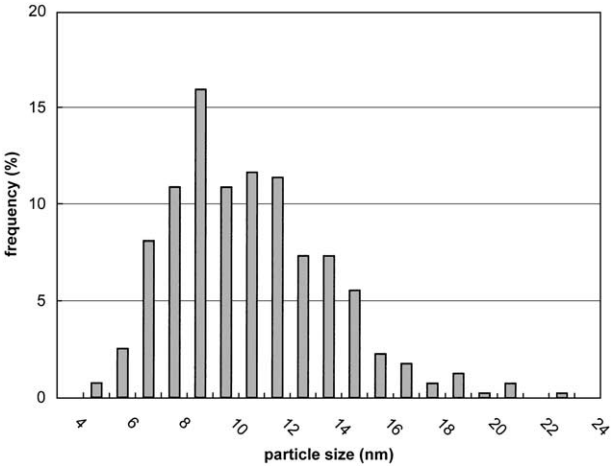

Fig. 3. Histogram of particle size frequencies. Merging of data from 5 samples. 395 particles measured (see text).

3.1.2. *Kinetics*

Estimated precipitation rates as defined by expression (2) are reported in Table 1. The rate of the overall reaction increases linearly as a function of TIC. A reaction order of 1 vs. TIC is deduced from a classical log-log plot (Fig. 4). Using Eqn. 1 and classical kinetics expression, this rate can also be written (in the log form) as follows:

$$\log R_m = \log k + 2n \log[Fe^{3+}] + m \log[Fe^{2+}] + 8q\ pH \quad (4)$$

where *n, m,* and *q* are the empirical partial orders of reaction for ferric, the ferrous ions, and the protons respectively. *n, m,* and *q* are natural integers; *k* is the rate constant of reaction, and *p*H is the *p*H of the solution. Since *p*H is constant in our experimental settings (*p*H = 10.5), and since $[Fe^{3+}] = 2/3\ TIC$ and $[Fe^{2+}] = 1/3\ TIC$, Eqn. 4 can be reduced to:

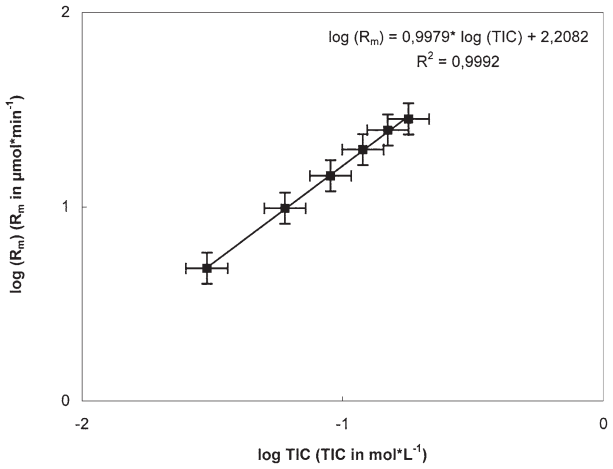

Fig. 4. Log-log plot of the measured reaction rate as a function of total iron concentration. Overprinted is a trend line of slope 1.00, therefore the results are consistent with a first-order rate law. R_m in μmol min^{-1} and TIC in mol.L^{-1}.

$$\log R_m = k' + (2n + m) \log TIC \quad (5)$$

where k' is a constant equal to $2n \log 2 - (2n + m) \log 3 + \log k + 8q$ *p*H. The quantity $(2n + m)$ is therefore the slope of the curve shown in Figure 4 that is close to a value of 1. Therefore, having $(2n + m) = 1$ gives only one solution with $n = 0$ and $m = 1$. This suggests that in presence of ferric and ferrous ions in solution, the magnetite formation is kinetically controlled by the activity of Fe^{2+}. This result is consistent with the observations of Jolivet et al. (1992) who showed that a ferric hydroxide was the first step of magnetite formation. In a second step, ferrous ions are added to the previously formed mineral to form the magnetite. This addition, which stabilizes the oxide structure, is the rate-determining step of the precipitation (Jolivet et al., 1994). A few seconds after stopping addition of iron to the solution, aliquots of solutions were sampled and TIC in these solutions was measured with GFAAS. Very small residual concentrations ($\sim 10^{-7}$ mol L^{-1}) were found, indicating that the precipitation is completed within short times.

3.1.3. Implications of mineralogical and kinetical results for the reaction pathway

Pure magnetite is thus synthesized within minutes in aqueous media with appropriate *p*H, with Fe(III)/Fe(II) ratio equal to 2, and at high TIC only. For lower TIC, other iron oxides such as goethite are formed and found to coexist with magnetites, the relative proportion of magnetite increasing with increasing TIC. Indeed, decreasing TIC in our experiments has similar effects as increasing Fe(III)/Fe(II) ratio as reported in previous experiments (Jolivet et al., 1992). As phases containing ferric ions are less soluble than those with ferrous ions, the clustering of Fe^{3+} under basic conditions is enhanced. At *p*H = 10.5, the precipitation of ferric ions is kinetically favored and might explain the preferential formation of Fe(III) oxides at the lowest TIC. Only once Fe(II) concentrations exceed some threshold, they can interact in the precipitation process leading to the formation of magnetite, possibly via a highly unstable intermediate phase which was not detected in the present study. This explanation could commonly apply to low TIC (this study) or to high Fe(III)/Fe(II) ratio (Jolivet et al., 1992). It would explain the measured rate law (Fig. 4) with the rate-determining step being the addition of Fe^{2+} to a rapidly formed transient precursor phase (e.g., ferrihydrite).

Precipitation from supersaturated solutions basically consists of two different processes: nucleation and growth. Far from equilibrium conditions, nucleation is the major implied process (Lasaga, 1998). The measured reaction rates and the absence of dependence of size on TIC strongly suggest that direct growth from the solution does not proceed in our experiments. This result is consistent with the model proposed by Jolivet et al. (1994), suggesting that at such *p*H, the effective interfacial tension between magnetite and water is small and even negative, thus suppressing driving forces for growth and Ostwald ripening. Indeed, the particle size is found to be independent of the quantity of solid precipitated material, of the total duration of one given experiment, as well as of the age of the material. Therefore, the first particles formed are not used as secondary nucleation sites. Because particles size does not change as a function of TIC, the nucleation process should be identical over the whole concentration range.

After identification of the possible reaction pathway, we noticed that the magnetite particles synthesized by inorganic processes obey some of the biogenicity criteria for biologically controlled magnetites (Bazylinski and Frankel, 2003) given for instance in Thomas-Keprta et al. (2000) (see Figs. 1 and 2). Some of the criteria, however, are not fulfilled. The crystals are not in the size range of single domain magnetites: they are much smaller. Moreover, we could not test the criteria of chemical purity and chain alignment, because no impurity was added in the medium and because a magnetic stirring was used during the precipitations. Further studies need to be performed for a detailed discussion. However, the fact that particles are nearly defect free and high crystallinity show that we have in this study an interesting inorganic model of nanocrystalline magnetites synthesis, which might provide important information about the reaction pathway of biogenic magnetite synthesis in magnetosomes.

3.2. Isotopic Fractionation

3.2.1. Magnetite–water oxygen isotope fractionation factors

The results of isotopic fractionation of oxygen measurements between magnetite and water are given in Table 1 and shown in Figure 5. For TIC $> 30 \times 10^{-3}$ mol L^{-1}, no fractionation of oxygen isotopes between magnetite and water can be evidenced within the analytical precision. On the other hand, for lower TIC, significant fractionations of oxygen isotopes between water and iron oxides are observed. This increase in oxygen isotope fractionation factor observed for TIC values lower than 30×10^{-3} mol L^{-1} may be due either to the presence of iron oxides other than magnetite, or to a dependence of the magnetite/water fractionation on TIC, or to a combination of both effects. Oxygen isotope fractionation between magnetite and water has been studied by several authors, at various temperatures, under abiotic or biotic conditions (Becker and Clayton, 1976; Blattner et al., 1983; Fortier et al., 1995; Mandernack et al., 1999; Zhang et al., 1997) (Fig. 5). At temperatures higher than 350°C, Fortier et al. (1995) obtained values of $10^3 ln\ \alpha_{m\text{-}e} = -8.47 \pm 0.23‰$ by laser fluorination technique and $10^3 ln\ \alpha_{m\text{-}w} = -8.60 \pm 0.65‰$ by ion microprobe analyses. Becker and Clayton (1976) have measured and calculated magnetite–water oxygen isotope equilibrium fractionation factors at lower temperatures. At 25°C, they obtained a calculated equilibrium fractionation factor of $10^3 ln\ \alpha_{m\text{-}w} = -4.66‰$, and the calculated values are always negative between 0 and 727 °C. On the other hand, magnetite biomineralization, which is known to occur in living organisms, chiton radula, newt, homing pigeon, and termites (Brassard et al., 1999; Chang and Kirschvink, 1989; Mielczarek and McGrayne, 2000; O'Neil and Clayton, 1964), seems to lead to close to zero or to positive fractionation factors. Positive magnetite–water fractionation has indeed been observed by O'Neil and Clayton (1964), who studied magnetites in radulae of *Cryptochito stelleri*. They found $10^3 ln\ \alpha_{m\text{-}w}$ of 5.6‰ for these biogenic crystals, suggesting strong kinetic effects in the isotope fractionation. These strong kinetic effects are suggested only if the theoretically calculated values for the fractionation factors at low temperature are correct. But since

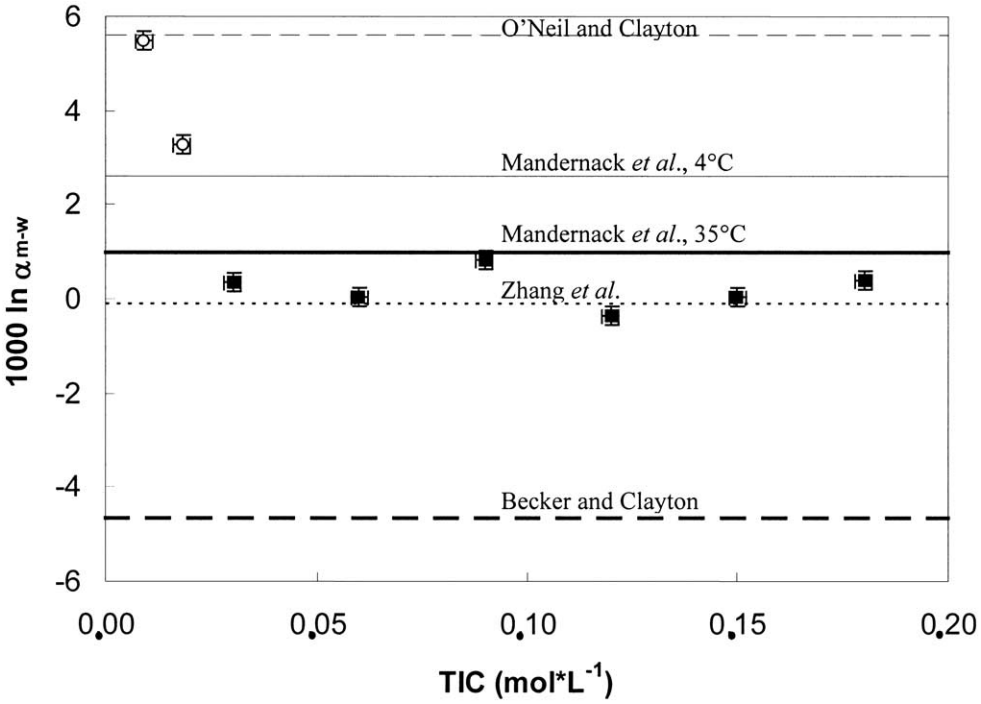

Fig. 5. Fractionation factor of ^{16}O and ^{18}O isotopes between water and iron oxide plotted as a function of total iron concentration. Solid squares: pure magnetite of this study. Below 0.030 mol.L^{-1}, iron oxides are not pure magnetite: open circles are then used. Previous literature studies did not specify total iron concentration and are thus shown as lines. Thin solid line: Mandernack et al. (1999) (4°C); thick solid line: Mandernack et al. (1999) (35°C); thin dotted line: Zhang et al. (1997) (biomagnetite 50°C); thin dashed line: O'Neil and Clayton (1964); thick dashed line: Becker and Clayton (1976) (25°C).

the accuracy of the low-temperature extrapolations of the theoretical value is unknown, the use of the theoretical predictions as baseline for confident assessments of kinetic vs. equilibrium oxygen isotope effects in low-temperature magnetite is problematic. Zhang et al. (1997) worked on magnetite formed by thermophilic iron-reducing bacteria. They measured values of $10^3 ln\ \alpha_{s\text{-}w}$ varied from −0.09‰ (50°C) to −1.08‰ (70°C) for biogenic samples and from 0.54‰ (50°C) to 1.24‰ (70°C) for control samples (without bacteria), indicating that the mineral–water fractionations in the controls were different from those in the enrichment cultures. However, control samples contained a mixture of poorly crystallized hematite and akagenite and therefore, although these latter inorganic fractionation values are compatible with those obtained in our study, it is not possible to compare them. In their study of magnetite particles produced by magnetotactic bacteria, Mandernack et al. (1999) reported values of $10^3 ln\ \alpha_{m\text{-}w}$ in the range +0.9 to 2.6‰. Once again, these values are comparable with ours. Mandernack et al. (1999) speculated that their values of $\delta^{18}O$ might indeed reflect temperature-dependent isotopic equilibrium.

3.2.2. Implications of isotopic results

It is worth noting that the results obtained on isotopic compositions of magnetites produced by bacteria, either extracellularly by thermophilic (45–75°C) iron-reducing bacteria (Zhang et al., 1997) or intracellularly by magnetotactic bacteria (Mandernack et al., 1999) exhibit very small magnetite/water fractionations, close to those observed in the present study. Our mineralogical, kinetic, and isotopic results thus indicate a reaction pathway for the formation of magnetite showing some similarities with the biogenic one (Frankel et al., 1983). Therefore, we suggest that the solution chemistry used for inorganic precipitation in this study is relevant to the conditions of magnetite precipitation in bacterially mediated processes such as magnetosome formation, particularly high saturation states, and perhaps *p*H.

It is also worth noting the discrepancy between isotopic results from literature at low temperature for magnetite–water fractionation. More studies should thus be devoted to measure low-temperature equilibrium fractionations between magnetite and water and to differentiate the kinetic vs. equilibrium oxygen isotope fractionation. It is important to notice that we have studied the fractionation of oxygen isotopes for different TIC and therefore for different supersaturation states. This is a new approach for the study of isotopic fractionation in general, which might be useful for the use of stable isotopes of biomarkers (Boschker and Middelburg, 2002).

4. CONCLUSIONS

Abiotic magnetite nanoparticles have been synthesized in aqueous media under constant controlled chemical affinity, at atmospheric pressure and temperature of 25°C. Other iron oxides were observed to coexist with magnetites for low TIC, whereas for higher TIC only magnetite particles were obtained.

Based on EELS, we have shown the precipitated nanocrystals to be magnetites and not maghemites. For those conditions where only magnetite is formed, crystal properties are the same for the whole range of supersaturation studied. Indeed, the size distribution of magnetite crystals does not depend on the TIC, in agreement with the model proposed by Jolivet et al. (1994). The kinetics of magnetite precipitation is related to TIC by a first-order rate law with respect to TIC. These results are explained by a model involving a first step of Fe(III) oxide or hydroxide formation, a second step of reaction of Fe(II) with this solid, and then rapid evolution to magnetite (Jolivet et al., 1992; Jolivet et al., 1994). Furthermore, the fractionation of oxygen isotopes between water and magnetite is found to be close to 0 for all samples in which only magnetite crystals were formed. This result is similar to observations in bacterial magnetites. Oxygen isotopic effects of the same order are thus occurring during bacterial precipitation of magnetites and during inorganic magnetite synthesis in aqueous medium at 25°C. The important implications of these results are that oxygen isotopic composition of low-temperature magnetite can not be directly used as a biosignature and that the solution chemistry used in this study for inorganic precipitation is relevant to better understanding of magnetite precipitation in bacterial magnetosomes, which might thus be characterized by high saturation states and *p*H. It would therefore be of great interest to be able to measure actual *p*H and TIC within bacterial magnetosomes or close to cellular surfaces of bacteria producing magnetites extracellularly, and to compare those measurements with the reference abiotic and inorganic results of the present study.

Acknowledgments—D. F. would like to thank M. Azaroual from the Bureau de Recherches Géologiques et Minières (BRGM) for introducing EQ3NR software and R. Hellmann from Laboratoire de Géophysique Interne et Minières (LGIT) for fruitful discussion. This research was, in part, financially supported by special programs (Bonus Qualité Recherche) from Institut de Physique du Globe de Paris (IPGP) and University of Paris 7. This paper greatly benefited from the valuable comments of an anonymous reviewer, B. Weiss and C. Yapp.

Associate editor: J. Horita

REFERENCES

Anbar A. D. (2001) Iron isotope biosignatures. Promise and progress. *EOS* **82** (*15*)**,** 173–179.

Anbar A. D. (2004) Iron stable isotopes: Beyond biosignatures. *Earth Planet. Sci. Lett.* **217,** 223–236.

Baeuerlein E. (2000) Biomineralization. Wiley-VCH, Weinheim.

Bao H. and Koch P. L. (1999) Oxygen isotope fractionation in ferric oxide-water system: Low temperature synthesis. *Geochim. Cosmochim. Acta* **63** (*5*)**,** 599–613.

Barber D. J. and Scott E. R. D. (2002) Origin of supposedly biogenic magnetite in the Martian meteorite Allan Hills 84001. *Proc. Natl. Acad. Sci. USA* **99** (*10*)**,** 6556–6561.

Bazylinski D. A. (1999) Synthesis of th bacterial magnetosome: The making of a magnetic personality. *Internatl. Microbiol.* **2,** 71–80.

Bazylinski D. A. and Frankel R. B. (2003) Biologically controlled mineralization in prokaryotes. In *Biomineralization,* Vol. 54 (eds. P. M. Dove, J. J. De Yoreao and S. Weiner), pp. 217–248. Mineralogical Society of America, Geochemical Society.

Bazylinski D. A., Frankel R. B., Heywood B. R., Mann S., King J. W., Donaghay P. L., and Hanson A. K. (1995) Controlled biomineralization of magnetite (Fe_3O_4) and greigite (Fe_3S_4) in a magnetotactic bacterium. *Appl. Environ. Microbiol.* **61** (*9*)**,** 3232–3239.

Beard B. L., Johnson C. M., Skulan J. L., Nealson K. H., Cox L., and Sun H. (2003) Application of Fe isotopes to tracing the geochemical and biological cycling of Fe. *Chem. Geol.* **195,** 87–117.

Becker R. H. and Clayton R. N. (1976) Oxygen isotope study of a Precambrian banded iron-formation. Hamersley Range. Western Australia. *Geochim. Cosmochim. Acta* **40,** 1153–1165.

Blake D., Treiman A. H., Cady S., Nelson C., and Krishnan K. (1998) Characterization of magnetite within carbonate in ALH84001. *Lunar Planet. Sci.* **XXIX,** Abstract #1347.

Blakemore R. P. (1975) Magnetotactic bacteria. *Science* **190,** 377–379.

Blakemore R. P., Maratea D., and Wolfe R. S. (1979) Isolation and pure culture of freshwater magnetic spirillum in chemically defined medium. *J. Bacteriol.* **140,** 720–729.

Blattner P., Braithwaite W. R., and Glover R. B. (1983) New evidence on magnetite oxygen isotope geothermometers at 175° and 112°C in Wairakei steam pipeline (New Zealand). *Isotope Geosci.* **1,** 195–204.

Boschker H. T. S. and Middelburg J. J. (2002) Stable isotopes and biomarkers in microbial ecology. *FEMS Microbiol. Ecol.* **40** (*2*)**,** 85–95.

Bradley J. P., Harvey R. P., McSween J. Y., McKay D. S., Gibson J. E., Thomas-Keprta K., and Vali H. (1997) No 'nanofossils' in martian meteorite. *Nature* **390,** 454–456.

Brantley S. L., Liermann L., and Bullen T. D. (2001) Fractionation of Fe isotopes by soil microbes and organic acids. *Geology* **29** (*6*)**,** 535–538.

Brassard J., Kirschvink J. L., Phillips J. B., and Borland S. C. (1999) Ferromagnetic material in the Eastern red-spotted newt. *Nophthalmus viridescens. J. Exp. Biol.* **202,** 3155–3160.

Bullen T. D., White A. F., Childs C. W., Vivit D. V., and Schultz M. S. (2001) Demonstration of significant abiotic iron isotope fractionation in nature. *Geology* **29** (*8*)**,** 699–702.

Chang S.-B. R. and Kirschvink J. L. (1989) Magnetofossils, the magnetization of sediments, and the evolution of magnetite biomineralization. *Ann. Rev. Earth Planet. Sci.* **17,** 169–195.

Clayton R. N. and Mayeda T. K. (1963) The use of bromine pentafloride in the extraction of oxygen from oxides and silicates for isotopic analysis. *Geochim. Cosmochim. Acta* **27,** 43–52.

Cornell R. M. and Schwertmann U. (1996) The Iron Oxides: Structure, Properties, Reactions, Occurrence and Uses. VCH, Weinheim.

Crocombette J. P., Pollack M., Jolet F., Thromat N., and Gautier-Soyer M. (1995) X-ray absorption spectroscopy at Fe L2,3 threshold in iron oxides. *Phys. Rev. B* **52,** 3143–3150.

Devouard B., Posfai M., Hua X., Bazylinski D. A., Frankel R. B., and Buseck P. B. (1998) Magnetite from magnetotactic bacteria: Size distributions and twinning. *Am. Min.* **83,** 1387–1398.

Fortier S. M., Cole D. R., Wesolowski D. J., Riciputi L. R., Paterson B. A., Valley J. W., and Horita J. (1995) Determination of the magnetite–water equilibrium oxygen isotope fractionation factor at 350°C: A comparison of ion microprobe and laser fluorination techniques. *Geochim. Cosmochim. Acta* **59,** 3871–3875.

Frankel R. B. and Blakemore R. (1979) Magnetite in freshwater magnetotactic bacteria. *Science* **203,** 1355–1356.

Frankel R. B. and Buseck P. B. (2000) Magnetite biomineralization and ancient life on Mars. *Curr. Opin. Chem. Biol.* **4,** 171–176.

Frankel R. B., Papaefthymiou G. C., Blakemore R. P., and O'Brian W. (1983) Fe_3O_4 precipitation in magnetotactic bacteria. *Biochim. Biophys. Acta* **763,** 147–159.

Friedmann E. I., Wierzchos J., Ascaso C., and Winklhofer M. (2001) Chains of magnetite crystals in the meteorite ALH84001: Evidence of biological origin. *Proc. Natl. Acad. Sci. USA* **98** (*5*)**,** 2176–2181.

Golden D. C., Ming D. W., Schwandt C. S., Lauer J. H. V., Socki R. A., Morris R. V., Lofgren G. E., and McKay G. A. (2001) A simple inorganic process for formation of carbonates, magnetite and sulfides in Martian meteorite ALH84001. *Am. Min.* **86,** 370–375.

Hochella M. F., Jr.. (2002) Nanoscience and technology: The next revolution in the Earth sciences. *Earth Planet. Sci. Lett.* **203,** 593–605.

Jolivet J. P., Belleville P., Tronc E., and Livage J. (1992) Influence of Fe(II) on the formation of the spinel iron oxide in alkaline medium. *Clays Clay Miner.* **40** (*5*)**,** 531–539.

Jolivet J. P., Henry M., and Livage J. (1994) De la solution à l'oxyde. CNRS Edition.

Kendelewicz T., Liu P., Doyle C. S., and Brown G. E. (2000a) Spectroscopic study of the reaction of aqueous Cr(VI) with Fe_3O_4 (111) surface. *Surf. Sci.* **469 (***2–3***),** 144–163.

Kendelewicz T., Liu P., Doyle C. S., Brown J. G. E., Nelson E. J., and Chambers S. A. (2000b) Reaction of water with the (100) and (111)surfaces of Fe_3O_4. *Surf. Sci.* **453,** 32–46.

Kirschvink J. L. (1982) Paleomagnetic evidence for fossil biogenic magnetite in western Crete. *Earth Planet. Sci. Lett.* **59,** 388–392.

Kirschvink J. L. and Chang S.-B. R. (1984) Ultrafine-grained magnetite in deep-sea sediments: Possible bacterial magnetofossils. *Geology* **12,** 559–562.

Kirschvink J. L. and Hagadorn J. W. (2000) A grand unified theory of biomineralization. In *The Biomineralization of Nano- and Micro-Structures* (ed. E. Bäuerlein), pp. 139–150. Wiley-VCH Verlag GmbH, Weinheim.

Krumbein W. E. (1983) Microbial Geochemistry. Blackwell Scientific Publications, Oxford.

Lasaga A. C. (1998) Kinetic Theory in the Earth Sciences. Princeton University Press, Princeton.

Mandernack K. W., Bazylinski D. A., Shanks W. C., and Bullen T. D. (1999) Oxygen and iron isotope studies of magnetite produced by magnetotactic bacteria. *Science* **285,** 1892–1896.

Mann S. and Hannington J. P. (1987) Formation of iron oxides in unilamellar vesicles. *J. Col. Interf. Sci.* **122 (***2***),** 326–335.

Mann S., Sparks N. H. C., Couling S. B., and Larcombe M. C. (1989) Crystallochemical characterization of magnetc spinels prepared from aqueous solution. *J. Chem. Soc., Faraday Transcript 1* **85 (***9***),** 3033–3044.

McCartney M. R., Lins U., Farina M., Buseck P. R., and Frankel R. B. (2001) Magnetic microstructure of bacterial magnetite by electron holography. *Eur. J. Min.* **13,** 685–689.

McKay D. S., Gibson E. K., Jr., Thomas-Keprta K. L., Vali H., Romanek C. S., Clemett S. J., Chilier X. D. F., Maechling C. R., and Zare R. N. (1996) Search for past life on mars: Possible relic biogenic in Martian meteorite ALH84001. *Science* **273,** 924–930.

Michard G. (1989) Equilibres chimiques dans les eaux naturelles. Editions Publisud, Paris.

Mielczarek E. V. and McGrayne S. B. (2000) Iron, Nature's Universal Element: Why People Need Iron & Animals Make Magnets. Rutgers University Press, New Brunswick, N.J.

Monceau D. and Boudias C. (1996) CaRIne cristallography. DIVERGENT S.A. Centre de Transfert.

Mortimer R. J. G. and Coleman M. L. (1997) Microbial influence on the oxygen isotopic composition of diagenetic siderite. *Geochim. Cosmochim. Acta* **61 (***8***),** 1705–1711.

Moskovitz B. M., Frankel R. B., and Bazylinski D. A. (1993) Rock magnetic criteria for the detection of biogenic magnetite. *Earth Planet. Sci. Lett.* **120,** 283–300.

Newman D. K. (2001) How bacteria respire minerals. *Science* **292,** 1312–1313.

O'Neil J. R. and Clayton R. N. (1964) Oxygen isotope geothermometry. In *Isotopic and Cosmic Chemistry* (ed. H. Craig), pp. 157–168. North Holland.

Qu S., Yang H., Ren D., Kan K., Zou G., Li D., and Li M. (1999) Magnetite nanoparticles prepared by precipitation from partially reduced ferric chloride aqueous solution. *J. Col. Interf. Sci.* **215,** 190–192.

Regazzoni A. E., Urrutia G. A., Blesa M. A., and Maroto A. J. G. (1981) Some observations on the composition and morphology of synthetic magnetites obtained by different routes. *J. Inorg. Nucl. Chem.* **43,** 1489–1493.

Roe J. E., Anbar A. D., and Barling J. (2003) Nonbiological fractionation of Fe isotopes: Evidence of an equilibrium isotope effect. *Chem. Geol.* **195,** 69–85.

Romanek C. S., Grady M. M., Wright I. P., Mittlefehldt D. W., Sockl R. A., Pillinger C. T., and Gibson J. E. K. (1994) Record of fluid–rock interactions on Mars from the meteorite ALH84001. *Nature* **372,** 655–657.

Schedin F., Morrall P., Petrov V. N., Case S., Thomas M. F., Dudzik E., Van der Laan G., and Thornton G. (2000) Magnetic properties of ultrathin epitaxial Fe_3O_4 films on Pt(1 1 1). *J. Magn. Magn. Mater* **211,** 266–270.

Schüler D. and Frankel R. B. (1999) Bacterial magnetosomes: Microbiology, biomineralization and biotechnological applications. *Appl. Microbiol. Biotechnol.* **52,** 464–473.

Schwertmann U. and Cornell R. M. (1991) Iron Oxides in the Laboratory: Preparation and Characterization. VCH, Weinheim.

Sweeton F. H. and Baes C. F., Jr.. (1970) The solubility of magnetite and hydrolysis of ferrous ion in aqueous solutions at elevated temperatres. *J. Chem. Thermodyn.* **2,** 479–500.

Taylor A. P., Barry J. C., and Webb R. I. (2001) Structural and morphological anomalies in magnetosomes: Possible biogenic origin for magnetite in ALH84001. *J. Microsc.* **201 (***1***),** 84–106.

Thomas-Keprta K. L., Bazlinski D. A., Kirschvink J. L., Clemett S. J., McKay D. S., Wentworth S. J., Vali H., Gibson E. K., Jr., and Romanek C. S. (2000) Elongated prismatic crystals in AL84001 carbonate globules: Potential Martian magnetofossils. *Geochim. Cosmochim. Acta* **64 (***23***),** 4049–4081.

Thomas-Keprta K. L., Clemett S. J., Bazlinski D. A., Kirschvink J. L., McKay D. S., Wentworth S. J., Vali H., Gibson E. K., Jr., McKay M. F., and Romanek C. S. (2001) Truncates hexa-octahedral magnetite crystals in ALH84001: Presumptive biosignature. *Proc. Natl. Acad. Sci. USA* **98 (***5***),** 2164–2169.

Tronc E., Belleville P., Jolivet J. P., and Livage J. (1992) Transformation of ferric hydroxide into spinel by Fe(II) adsorption. *Langmuir* **8,** 313–319.

Vali H., Forster O., Amarantidid G., and Petersen H. (1987) Magnetotactic bacteria and their magnetofossils in sediments. *Earth Planet. Sci. Lett.* **86,** 389–400.

Vali H. and Kirschvink J. L. (1989) Magnetofossil dissolution in a paleomagnetically unstable deep-sea sediment. *Nature* **339,** 203–206.

Vayssières L. (1995) Précipitation en milieu aqueux de nanoparticules d'oxydes. Modélisation de l'interface et contrôle de la croissance. University P. et M. Curie, Paris 6, Paris.

Vayssières L., Chanéac C., Tronc E., and Jolivet J. P. (1998) Size tailoring or magnetite particles formed by aqueous precipitation: An example of thermodynamic stability of nanometric oxide particles. *J. Col. Interf. Sci.* **205,** 205–212.

Wolery T. J. (1979) Calculations of chemical equilibrium between solutions and minerals: The E3/6 Software Package: UCRL-52658. Lawrence Livermore National Laboratory, Livermore, California.

Yapp C. J. (1987) Oxygen and hydrogen isotope variations among goethites (a-FeOOH) and the determination of paleotemperatures. *Geochim. Cosmochim. Acta* **51 (***2***),** 355–364.

Zhang C., Liu S., Phelps T. J., Cole D. R., Horita J., Fortier S. M., Elless M., and Valley J. W. (1997) Physiochemical, mineralogical, and isotopic characterization of magnetite-rich iron oxides formed by thermophilic iron-reducing bacteria. *Geochim. Cosmochim. Acta* **61 (***21***),** 4621–4632.